Research in Astron. Astrophys. **2009** Vol. **9** No. **11**, 1192–1204
http://www.raa-journal.org *http://www.iop.org/journals/raa*

***R**esearch in*
***A**stronomy and*
***A**strophysics*

SDSS spectroscopy for blazars in the *Fermi* LAT bright AGN sample *

Zhao-Yu Chen[1,2], Min-Feng Gu[1], Zhong-Hui Fan[3] and Xin-Wu Cao[1]

[1] Key Laboratory for Research in Galaxies and Cosmology, Shanghai Astronomical Observatory, Chinese Academy of Sciences, Shanghai 200030, China; *zychen@shao.ac.cn*
[2] Graduate University of Chinese Academy of Sciences, Beijing 100049, China
[3] Department of Physics, Yunnan University, Kunming 650091, China

Received 2009 May 5; accepted 2009 June 18

Abstract We have collected all available spectra and photometric data from the SDSS catalog for bright AGNs complied from the first three months of the *Fermi* large area telescope all-sky survey. Based on the 106 high-confidence and 11 low-confidence associated bright AGN list, the photometry data are collected from SDSS DR7 for 28 sources (12 BL Lacs and 16 FSRQs), two of which are low-confidence associated bright AGNs. Among these 28 SDSS photometric sources, SDSS spectra are available for 20 sources (6 BL Lacs and 14 FSRQs). The black hole masses $M_{\rm BH}$ and the broad line region (BLR) luminosity were obtained for 14 FSRQs by measuring the line-widths and strengths of broad emission lines from the SDSS spectra. The broad emission line measurements of five FSRQs are presented for the first time in this work. The optical continuum emission of these 14 FSRQs is found to be likely dominated by the non-thermal jet emission by comparing the relationship between the broad Mg II line and continuum luminosity to that of radio-quiet AGNs. The black hole mass of the 14 FSRQs ranges from $10^{8.2}\,M_{\odot}$ to $10^{9.9}\,M_{\odot}$, with most of the sources larger than $10^{9}\,M_{\odot}$. The Eddington ratio $L_{\rm bol}/L_{\rm Edd}$ ranges from $10^{-1.5}$ to ~ 1. This implies that an optically thin, geometrically thick accretion disk may exist in these FSRQs.

Key words: galaxies: active — galaxies: nuclei — gamma rays: observations — quasars: emission lines — BL Lacertae objects: general

1 INTRODUCTION

Blazars, including BL Lac objects and flat-spectrum radio quasars (FSRQs), are the most extreme class of active galactic nuclei (AGNs), characterized by strong and rapid variability, high polarization, and apparent superluminal motion. These extreme properties are generally interpreted to be a consequence of non-thermal emission from a relativistic jet oriented close to the line of sight. As such, they represent a fortuitous natural laboratory with which to study the physical properties of jets, and, ultimately, the mechanisms of energy extraction from the central supermassive black holes.

The most prominent characteristic of the overall spectral energy distribution (SED) of blazars is the double-peak structure with two broad spectral components. The first, lower frequency component is generally interpreted as being due to synchrotron emission, and the second, higher frequency one

* Supported by the National Natural Science Foundation of China.

as being due to inverse Compton emission. BL Lac objects (BL Lacs) usually have no or only very weak emission lines, but have a strong highly variable and polarized non-thermal continuum emission ranging from the radio to γ-ray band, and their jets have synchrotron peak frequencies ranging from IR/optical to UV/soft-X-ray energies. Compared to BL Lacs, FSRQs have strong narrow and broad emission lines; however, they generally have low synchrotron peak frequency. According to the synchrotron peak frequency, BL Lac objects can be divided into three subclasses, i.e. low frequency peaked BL Lac objects (LBL), intermediate objects (IBL) and high frequency peaked BL Lac objects (HBL) (Padovani & Giommi 1995).

Although a point of agreement about the second component is that the γ-rays of blazars are produced in relativistic jets by inverse Compton scattering, the origin of the seed photons (optical/IR), the location and size of the emitting region, and the degree of relativistic beaming of the high-energy radiation, are all still unknown. Seed photons may come from the jet itself (Synchrotron Self-Compton model, SSC), from an accretion disk around a supermassive black hole at the base of the jet, or else from photons of the broad emission line region (e.g. Wehrle et al. 1998; Collmar et al. 2000). If the γ-rays originate from up-scattering of broad emission line photons, a correlation between the γ-rays and the emission lines would be expected. However, a direct comparison shows that there is no evidence of a correlation between the γ-rays and broad emission line luminosity (Fan 2000), likely due to the lack of line data. By estimating the energy density in the relativistic jet blobs contributed by the broad line region (BLR), Fan et al. (2006) claimed that the γ-ray emission can be from external Compton scattering, especially with seed photons from the broad line region. In the model fitting to SED including γ-ray emission, the external Compton processes have been taken into account in combination with SSC (Ghisellini et al. 1998; Ghisellini & Tavecchio 2008). The measurements of broad emission lines can be used to constrain the energy density of BLR in jets, although it also depends on the location of the jet region. On the other hand, the measurements of prominent broad emission lines, especially Hβ, Mg II and C IV, enable us to measure the black hole mass and the bolometric luminosity using various empirical relations, from which the accretion mode can be investigated.

The *Gamma-ray Large Area Space Telescope (GLAST)* was launched on 2008 June 11, and renamed the *Fermi Gamma-Ray Space Telescope* shortly after entering its scientific operating mission, which began on 2008 August 11. Abdo et al. (2009a) have presented a list of 116 bright, $\gtrsim 10\sigma$ sources at $|b| \geq 10^\circ$ taken from the list of bright sources (Abdo et al. 2009b) observed with the *Fermi* Large Area Telescope (LAT) in its initial three-month observing period extending from August 4 to October 30 of 2008. Of these sources, 106 are associated with blazars with high confidence and comprise the LAT Bright AGN Sample (LBAS). It contains two radio galaxies, namely Centaurus A and NGC 1275, and 104 blazars consisting of 57 FSRQs, 42 BL Lac objects, and 5 blazars with uncertain classification. The number of low-confidence AGN associations is 11 (one source having two possible associations — one high- and one low-confidence). In this work, we search the SDSS photometry and spectroscopy data for all these 116 AGNs, and results focussing on the spectral line analysis are shown. The cosmological parameters $H_0 = 70\,\mathrm{km\,s^{-1}\,Mpc^{-1}}$, $\Omega_m = 0.3$, and $\Omega_\Lambda = 0.7$ are used throughout the paper, and the spectral index α is defined as $f_\nu \propto \nu^{-\alpha}$ with f_ν being the flux density at frequency ν.

2 SDSS DATA ANALYSIS

The Sloan Digital Sky Survey (SDSS)[1] consists of a series of three interlocking imaging and spectroscopic surveys (Legacy, SEGUE, and Supernova), carried out over an eight-year period with a dedicated 2.5m telescope located at the Apache Point Observatory in Southern New Mexico. The seventh data release (DR7) from the SDSS represents the completion of this project. The DR7 imaging data cover about 8423 square degrees of "legacy" sky, with information on roughly 230 million distinct photometric objects, and about 3240 square degrees of SEGUE sky, with about 127 million distinct objects (including many stars at low latitude). The DR7 spectroscopic data include data from 1802 main survey plates of 640 spectra each, and cover 8200 square degrees. In addition, DR7 contains 762 "extra" and "special" plates.

[1] *http://www.sdss.org*

Table 1 *Fermi*-detected AGNs in SDSS

LAT Name (1)	Other Name (2)	SDSS Name (3)	Class (4)	z (5)	SDSS data (6)
0FGL J0050.5–0928	PKS 0048–097	J005041.31–092905.1	BLLac	0.537	PS
0FGL J0738.2+1738	PKS 0735+178	J073807.39+174218.9	BLLac	0.424	P
0FGL J0818.3+4222	OJ +425	J081815.99+422245.4	BLLac	0.530	PS
0FGL J0824.9+5551	TXS 0820+560	J082447.24+555242.6	FSRQ	1.417	PS
0FGL J0909.7+0145^L	PKS 0907+022	J090939.84+020005.2	BLLac	1.575	PS
0FGL J0921.2+4437	RGB J0920+446	J092058.46+444154.0	FSRQ	2.190	PS
0FGL J0948.3+0019	PMN J0948+0022	J094857.33+002225.5	FSRQ	0.585	PS
0FGL J0957.6+5522	4C +55.17	J095738.19+552257.7	FSRQ	0.896	PS
0FGL J1015.2+4927	1ES 1011+496	J101504.14+492600.6	BLLac	0.212	PS
0FGL J1015.9+0515	PMN J1016+0512	J101603.14+051302.3	FSRQ	1.715	PS
0FGL J1034.0+6051	S4 1030+61	J103351.42+605107.3	FSRQ	1.401	PS
0FGL J1057.8+0138	PKS 1055+018	J105829.60+013358.8	FSRQ	0.888	PS
0FGL J1058.9+5629	RX J10586+5628	J105837.73+562811.1	BLLac	0.143	PS
0FGL J1104.5+3811	Mrk 421	J110427.31+381231.7	BLLac	0.030	P
0FGL J1159.2+2912	4C +29.45	J115931.84+291443.8	FSRQ	0.724	PS
0FGL J1218.0+3006	B2 1215+30	J121752.08+300700.6	BLLac	0.130	P
0FGL J1221.7+2814	W Com	J122131.69+281358.4	BLLac	0.102	PS
0FGL J1229.1+0202	3C 273	J122906.69+020308.5	FSRQ	0.158	P
0FGL J1310.6+3220	B2 1308+32	J131028.66+322043.7	FSRQ	0.997	PS
0FGL J1427.1+2347	PKS 1424+240	J142700.39+234800.0	BLLac	...	P
0FGL J1504.4+1030	PKS 1502+106	J150424.98+102939.1	FSRQ	1.839	PS
0FGL J1522.2+3143	TXS 1520+319	J152209.99+314414.3	FSRQ	1.487	P
0FGL J1553.4+1255	PKS 1551+130	J155332.69+125651.7	FSRQ	1.290	PS
0FGL J1555.8+1110	PG 1553+11	J155543.04+111124.3	BLLac	0.360	P
0FGL J1635.2+3809	4C +38.41	J163515.50+380804.4	FSRQ	1.813	PS
0FGL J1641.4+3939^L	B3 1640+396	J164147.54+393503.3	FSRQ	0.539	PS
0FGL J1653.9+3946	Mrk 501	J165352.21+394536.6	BLLac	0.033	P
0FGL J2229.8–0829	PHL 5225	J222940.09–083254.5	FSRQ	1.560	PS

Notes: Col. (1): source LAT name. ^{L} represents low-confidence association AGNs. Col. (2): source other name. Col. (3): source SDSS name. Col. (4): class. Col. (5): redshift from NED. Col. (6): available SDSS data — P for photometry and S for spectroscopy.

Based on the 106 high-confidence associated and 11 low-confidence associated bright AGN list, the photometry data are collected from SDSS DR7 for 28 sources (12 BL Lacs and 16 FSRQs), listed in Table 1. Two out of 28 objects are low-confidence associated bright AGNs, i.e. BL Lac object 0FGL J0909.7+0145 identified with SDSS J090939.84+020005.2 ($z = 1.575$), and FSRQ 0FGL J1641.4+3939 associated with SDSS J164147.54+393503.3 ($z = 0.539$). Among these 28 SDSS photometric sources, SDSS spectra are available for 20 sources (6 BL Lacs and 14 FSRQs). Below, we present the data analysis based on the available SDSS data.

2.1 Photometry

SDSS DR7 provides an imaging catalog of 357 million unique objects, from which the magnitudes are available at $ugriz$ wavebands with average wavelengths 3551, 4686, 6165, 7481 and 8931 Å, respectively. As blazars often appear as point-like sources (although the faint host galaxy can be seen for BL Lac objects in some cases), the PSF magnitudes from SDSS are collected for all 28 sources, and are determined by fitting a PSF model to the object (see Table 2). The SDSS $ugriz$ magnitudes were firstly transferred to AB $ugriz$ magnitudes using the zeropoint offset between the SDSS system and the AB system (Oke & Gunn 1983), i.e. $u_{\rm AB} = u_{\rm SDSS} - 0.04$ mag, $g_{\rm AB} \sim g_{\rm SDSS}$, $r_{\rm AB} \sim r_{\rm SDSS}$, $i_{\rm AB} \sim i_{\rm SDSS}$ and $z_{\rm AB} = z_{\rm SDSS} + 0.02$ mag. Galactic extinctions are then corrected using the extinction law of Schlegel et al. (1998) and the $E(B-V)$ provided in the NASA/IPAC Extragalactic Database

Table 2 SDSS photometry

SDSS Name	u	g	r	i	z	$E(B-V)$	α_ν	$\log L_{5100\,\text{Å}}$ (erg s^{-1})
(1)	(2)	(3)	(4)	(5)	(6)	(7)	(8)	(9)
J005041.31-092905.1	16.77	16.39	16.05	15.80	15.57	0.032	1.03	45.93
J073807.39+174218.9	16.45	15.91	15.49	15.17	14.88	0.035	1.38	45.93
J081815.99+422245.4	19.20	18.61	18.08	17.71	17.38	0.063	1.55	45.18
J082447.24+555242.6	18.52	18.36	18.08	17.92	17.88	0.063	0.43	45.99
J090939.84+020005.2^L	20.37	19.88	19.53	19.18	18.98	0.031	1.24	45.76
J092058.46+444154.0	18.68	18.06	17.91	17.72	17.42	0.021	1.02	46.68
J094857.33+002225.5	18.96	18.60	18.44	18.19	18.18	0.079	0.48	45.05
J095738.19+552257.7	18.26	17.92	17.57	17.38	17.20	0.009	0.99	45.81
J101504.14+492600.6	15.71	15.43	15.23	15.11	14.96	0.012	0.64	45.28
J101603.14+051302.3	20.50	19.88	19.48	19.07	18.75	0.026	1.58	46.00
J103351.42+605107.3	19.31	18.88	18.46	18.17	17.93	0.010	1.30	46.04
J105829.60+013358.8	18.84	18.30	17.85	17.47	17.12	0.027	1.56	45.85
J105837.73+562811.1	16.92	16.50	16.00	15.73	15.49	0.012	1.36	44.57
J110427.31+381231.7	14.80	13.81	13.10	12.81	12.54	0.015	2.14	44.19
J115931.84+291443.8	18.75	18.21	18.08	17.95	17.68	0.019	0.85	45.39
J121752.08+300700.6	15.92	15.49	15.14	14.92	14.76	0.024	1.03	44.85
J122131.69+281358.4	15.84	15.39	15.05	14.78	14.58	0.023	1.13	44.67
J122906.69+020308.5	13.87	12.99	12.88	12.64	13.24	0.021	0.61	45.88
J131028.66+322043.7	18.40	18.02	17.61	17.34	17.12	0.014	1.20	45.97
J142700.39+234800.0	15.25	14.87	14.55	14.31	14.12	0.059	0.88	...
J150424.98+102939.1	18.90	18.52	18.22	17.84	17.59	0.032	1.15	46.45
J152209.99+314414.3	20.62	20.18	19.79	19.51	19.43	0.024	1.10	45.52
J155332.69+125651.7	17.50	17.40	17.24	17.20	17.17	0.042	0.16	46.14
J155543.04+111124.3	15.08	14.74	15.40	14.13	13.94	0.052	0.84	46.10
J163515.50+380804.4	17.77	17.67	17.63	17.38	17.26	0.011	0.42	46.40
J164147.54+393503.3^L	20.09	19.65	19.64	19.23	19.16	0.014	0.81	44.50
J165352.21+394536.6	15.36	13.85	13.04	12.62	12.32	0.019	2.86	44.24
J222940.09–083254.5	17.87	17.44	17.07	16.74	16.48	0.051	1.16	46.74

Notes: Col. (1): SDSS name. ^{L} represents low-confidence association AGNs. Cols. (2)–(6): SDSS five-band PSF magnitude $ugriz$. Col. (7): $E(B-V)$ from NED. Col. (8): the spectral index α_ν from power-law fit on u, g, r, i, z. Col. (9): luminosity at 5100 Å.

(NED)[2]. Finally, the flux density can be calculated from magnitudes at each waveband of $ugriz$ as:

$$S_\nu = 3631 \times 10^{-0.4m}\ \text{Jy} \tag{1}$$

in which S_ν and m are the flux density and Galactic extinction corrected AB magnitude at $ugriz$ wavebands, respectively. The simple power-law $S_\nu = a\nu^{-\alpha_\nu}$ is used to fit the flux density at $ugriz$ wavebands. The spectral index α_ν is presented in Table 2, in which the luminosity at 5100 Å calculated from the power-law fit is also given.

2.2 Spectral Analysis

The SDSS spectra cover a wavelength range from 3800 to 9200 Å with a resolution of about 1800–2200. In the first step, the SDSS spectra for all 20 sources were corrected for Galactic extinction using the reddening map of Schlegel et al. (1998) and then shifted to their rest wavelengths, adopting the redshifts (from NED) listed in Table 1.

2.2.1 BL Lac objects

Historically, an object is classified as a BL Lac object based on a flat radio spectrum ($\alpha_\nu \leq 0.5$) and an optical spectrum with emission lines weaker than a 5 Å rest-frame equivalent width, e.g. for the 1-Jy

[2] *http://nedwww.ipac.caltech.edu/*

Table 3 BL Lacs with SDSS spectra

SDSS Name	α_λ	$\log L_{5100\,\mathring{\mathrm{A}}}$ $(\mathrm{erg\,s^{-1}})$
(1)	(2)	(3)
J005041.31–092905.1	0.69	46.19
J081815.99+422245.4	0.79	45.00
J090939.84+020005.2^L	1.05	46.63
J101504.14+492600.6	1.32	45.37
J105837.73+562811.1	0.87	44.69
J122131.69+281358.4	0.86	44.85

Notes: Col. (1): SDSS name. ^{L} represents low-confidence association AGNs. Col. (2): the spectral index α_λ from power-law fit to SDSS spectra. Col. (3): luminosity at 5100Å.

radio survey (Stickel et al. 1991; Rector & Stocke 2001). The latter criterion was chosen to separate BL Lacs from FSRQ. However, this classification caused controversy. Later, the absorption feature which is the Ca H&K break was proposed in BL Lac classification in combination with the criterion of no or very weak emission lines in the optical spectrum (Marchã et al. 1996; see also Landt et al. 2002). In this work, we follow the BL Lac identification in Abdo et al. (2009a) (see their tables 1 and 2).

The SDSS spectra of 6 BL Lacs are featureless, and the Ca H&K break is not evident. Therefore, we use a single power-law to fit the spectral continuum, and the contribution of the host galaxy is ignored. The spectral index is shown in Table 3, as well as the luminosity at 5100 Å calculated from the fitted power-law.

2.2.2 FSRQs

The spectra of quasars are characterized by various broad and narrow emission lines (Vanden Berk et al. 2001). The redshifts of our 14 FSRQs range from 0.539 to 2.189 (see Table 1), with several broad emission lines apparently seen from the SDSS spectra, e.g. Hβ, Mg II and C IV lines (see Fig. 1). For our FSRQs sample, we ignore the host galaxy contribution to the spectrum, since only very little, if any, starlight is observed. In order to reliably measure line parameters, we choose those wavelength ranges as pseudo-continua, which are not affected by prominent emission lines, and then decomposed the spectra into the following three components (see also Chen et al. 2009):

1. A power-law continuum to describe the emission from the active nucleus. The 13 line-free spectral regions were firstly selected from SDSS spectra covering 1140 to 5630 Å for our sample, namely, 1140 – 1150 Å, 1275 – 1280 Å, 1320 – 1330 Å, 1455 – 1470 Å, 1690 – 1700 Å, 2160 – 2180 Å, 2225 – 2250 Å, 3010 – 3040 Å, 3240 – 3270 Å, 3790 – 3810 Å, 4210 – 4230 Å, 5080 – 5100 Å, and 5600 – 5630 Å (Vanden Berk et al. 2001; Forster et al. 2001). Depending on the source redshift, the spectrum of an individual quasar only covers some of them, from which the initial single power-laws are obtained for each source.
2. A Fe II template. The spectra of our sample cover UV and optical regions, therefore, we adopt the UV Fe II template from Vestergaard & Wilkes (2001), and the optical one from Véron-Cetty et al. (2004). For the sources with both UV Fe II and optical Fe II lines prominent in the spectra, we connect the UV and optical templates into one template covering the whole spectrum (see also Chen et al. 2009). In the fitting, we assume that Fe II has the same profile as the relevant broad lines, i.e. the Fe II line width was usually fixed to the line width of broad Hβ or Mg II or C IV, which in most cases gave a satisfying fit. In some special cases, a free-varying line width was adopted in the fitting to get better fits.
3. A Balmer continuum was generated in the same way as Dietrich et al. (2002) (see also Chen et al. 2009). Grandi (1982) and Dietrich et al. (2002) proposed that a partially optically thick cloud with

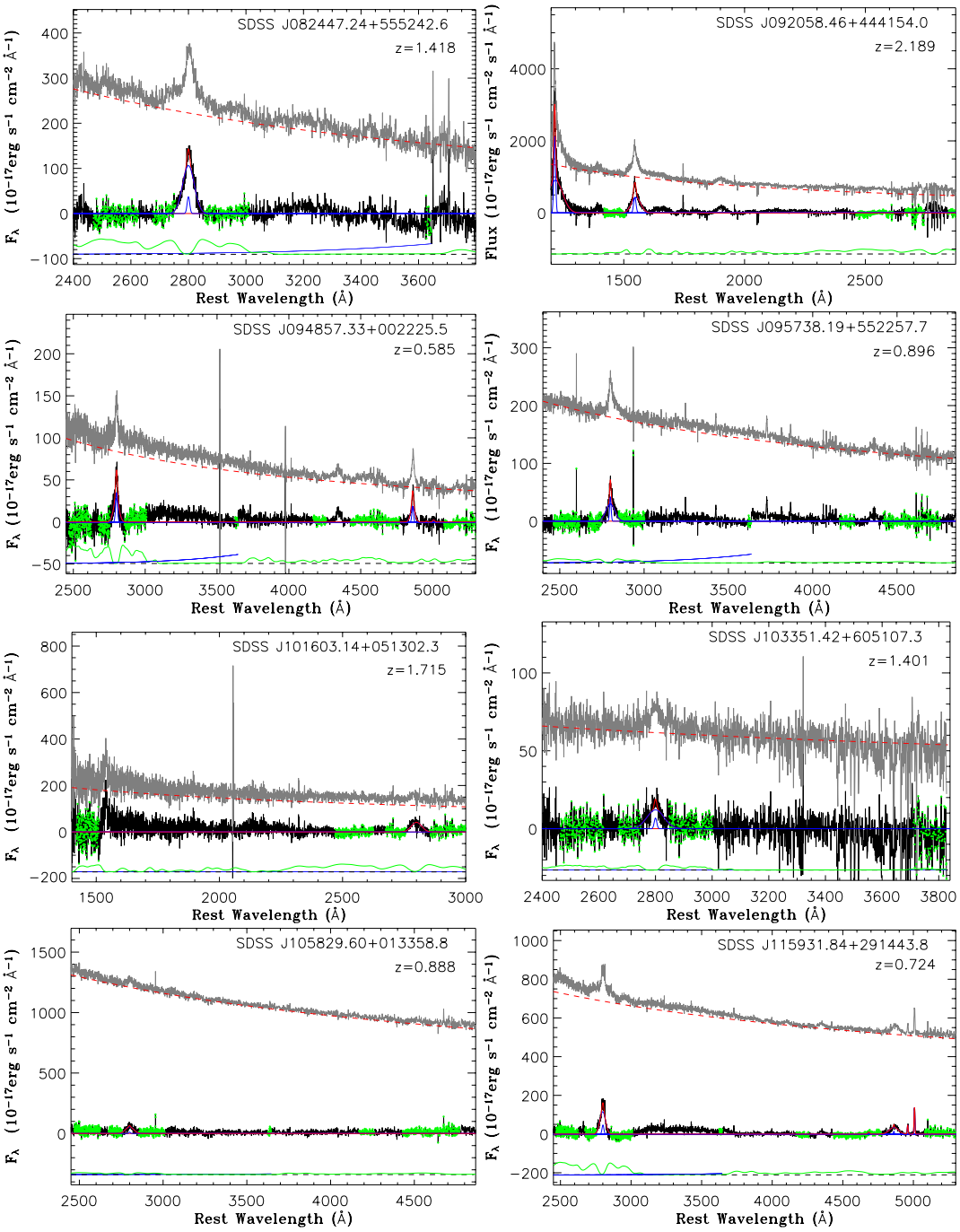

Fig. 1 Spectral analysis. The source SDSS name and redshift are presented in each panel in sequences of increasing source R.A. For each source panel, the top and middle grey lines are the original and the continuum-subtracted spectrum, respectively. The top dashed red line represents the power-law continuum. The middle blue lines are the individual line components in multi-line spectral fitting, and the middle solid red line is the integrated line fitting. The green spectral region in the continuum-subtracted spectrum is used to fit Fe II emission and power-law continuum, and the bottom green line is Fe II emission, which is shifted downwards with arbitrary units for the sake of presentation. When necessary, the Balmer continuum is indicated as solid blue lines in the bottom of each panel, which begins at the Balmer edge 3646 Å.

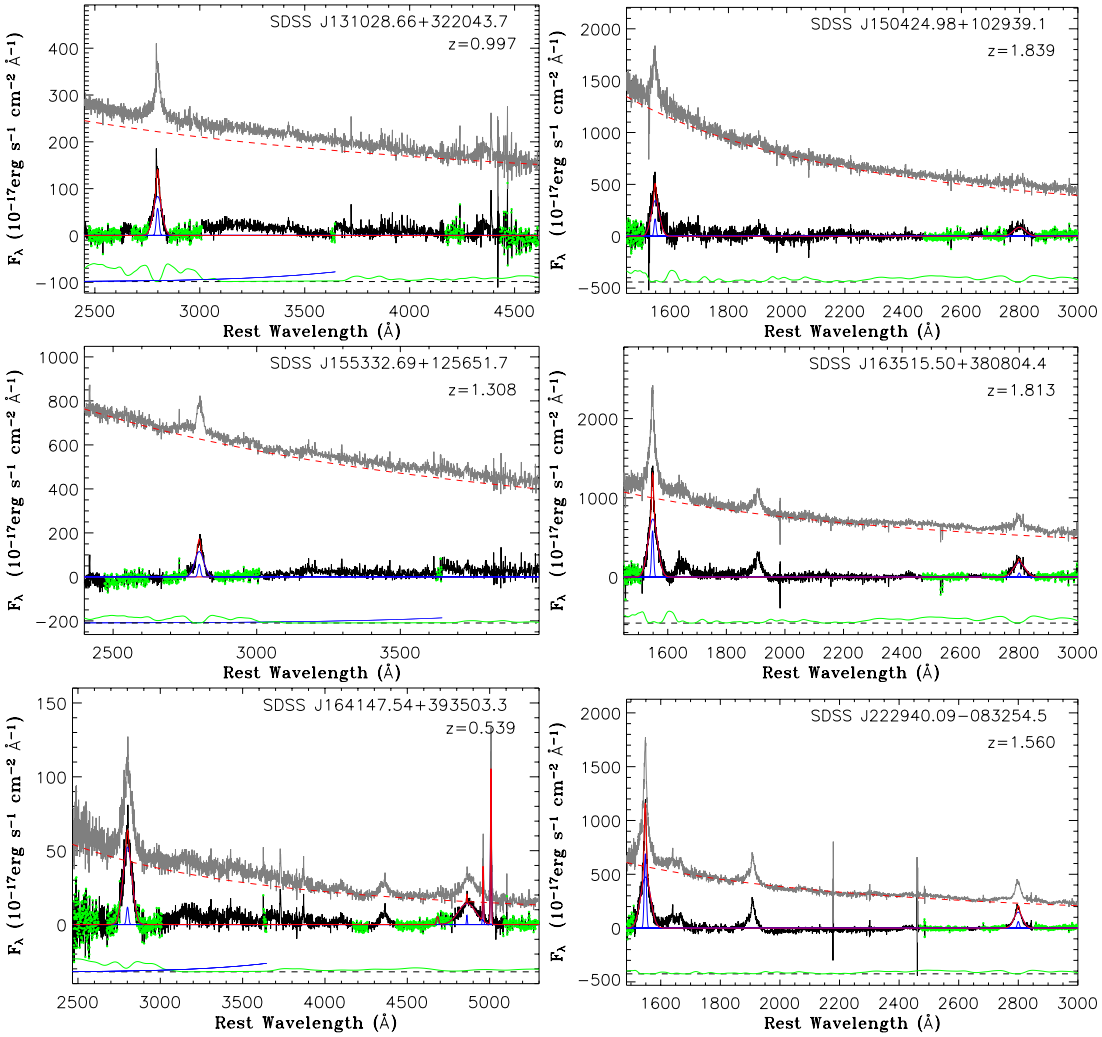

Fig. 1 —*Continued.*

a uniform temperature could produce the Balmer continuum, which can be expressed as:

$$F_{\lambda}^{\rm BaC} = F_{\rm BE} B_{\lambda}(T_{\rm e})(1 - e^{-\tau_{\lambda}}); \qquad (\lambda < \lambda_{\rm BE})\,, \tag{2}$$

where $F_{\rm BE}$ is a normalized coefficient for the flux at the Balmer edge ($\lambda_{\rm BE} = 3646$ Å), $B_{\lambda}(T_{\rm e})$ is the Planck function at an electron temperature $T_{\rm e}$, and τ_{λ} is the optical depth at λ and is expressed as:

$$\tau_{\lambda} = \tau_{\rm BE}\left(\frac{\lambda}{\lambda_{\rm BE}}\right), \tag{3}$$

where $\tau_{\rm BE}$ is the optical depth at the Balmer edge. There are two free parameters, $F_{\rm BE}$ and $\tau_{\rm BE}$. Following Dietrich et al. (2002), we adopt the electron temperature to be $T_{\rm e} = 15\,000$ K.

The modeling of the above three components is performed by minimizing the χ^2 in the fitting process. The final multicomponent fit is then subtracted from the observed spectrum. The fitted power-law, Fe II lines, Balmer continuum and the residual spectra for each source are shown in Figure 1. The Fe II fitting windows are selected as the regions with prominent Fe II line emission but no other strong

Table 4 Broad Emission Line Measurements for FSRQs

SDSS Name	C IV		Mg II		Hβ		α_λ	log $L_{3000\,\text{Å}}$
	FWHM ($\mathrm{km\ s^{-1}}$)	log F	FWHM ($\mathrm{km\ s^{-1}}$)	log F	FWHM ($\mathrm{km\ s^{-1}}$)	log F		($\mathrm{erg\ s^{-1}}$)
(1)	(2)	(3)	(4)	(5)	(6)	(7)	(8)	(9)
J082447.24+555242.6*	...	...	5119	–13.27	...	...	1.39	46.88
J092058.46+444154.0	8788	–12.68	...	...	...	...	1.18	47.69
J094857.33+002225.5*	...	...	4743	–13.89	2209	–14.15	1.28	45.50
J095738.19+552257.7	...	...	6709	–13.70	...	...	0.93	46.30
J101603.14+051302.3*	...	...	5268	–13.66	...	...	0.75	46.99
J103351.42+605107.3	...	...	7607	–14.04	...	...	0.43	46.34
J105829.60+013358.8	...	...	6214	–13.48	...	...	0.61	46.38
J115931.84+291443.8	...	...	5008	–13.24	4636	–13.56	0.52	46.67
J131028.66+322043.7	...	...	5278	–13.36	3633	–14.40	0.76	46.51
J150424.98+102939.1	6627	–12.90	5172	–13.35	...	...	1.69	47.44
J155332.69+125651.7*	...	...	3999	–13.34	...	...	1.28	47.24
J163515.50+380804.4	7452	–12.52	5144	–13.04	...	...	1.08	47.52
J164147.54+393503.3^L	...	...	7064	–13.44	7731	–13.72	1.84	45.11
J222940.09-083254.5*	7753	–12.69	3689	–13.27	...	...	1.53	46.81

Col. (1): SDSS name. * for sources with BLR data not available in the literatures and newly measured in this paper.^{L} represents low-confidence association AGNs. Col. (2): FWHM of broad C IV. Col. (3): flux of broad C IV in units of $\mathrm{erg\ s^{-1}\ cm^{-2}}$. Col. (4): FWHM of broad Mg II. Col. (5): flux of broad Mg II in units of $\mathrm{erg\ s^{-1}\ cm^{-2}}$. Col. (6): FWHM of broad Hβ. Col. (7): flux of broad Hβ in units of $\mathrm{erg\ s^{-1}\ cm^{-2}}$. Col. (8): the continuum spectral index α_λ from SDSS spectra. Col. (9): luminosity at 3000Å.

emission lines, according to Vestergaard & Wilkes (2001) and Kim et al. (2006). The fitting window around the Balmer edge (3625 – 3645 Å) is used to measure the contribution of the Balmer continuum, which extends to the Mg II line region. The Balmer continuum is not considered when 3625–3645 Å is out of the spectrum.

The broad emission lines were measured from the continuum subtracted spectra. We mainly focused on several prominent emission lines, i.e. Hβ, Mg II, and C IV. Generally, two Gaussian components were adopted to fit each of these lines, indicating broad and narrow line components, respectively. The blended narrow lines, e.g. [O III] $\lambda\lambda 4959, 5007$ Å and [He II] $\lambda 4686$ Å blending with Hβ were included as one Gaussian component for each line at the fixed line wavelength. The χ^2 minimization method was used in fits. The line width FWHM line flux of broad Hβ, Mg II and C IV lines were obtained from the final fits for our sample, and are listed in Table 4. The spectral fitting for each source is shown in Figure 1.

2.3 $M_{\rm bh}$ and $L_{\rm BLR}$

There are various empirical relations between the radius of the broad line region (BLR) and the continuum luminosity, which can be used to calculate the black hole mass in combination with the line width FWHM of broad emission lines. However, there are defects when using the continuum luminosity to estimate the BLR radius for blazars since the continuum fluxes of blazars are usually Doppler boosted due to the fact that the relativistic jet is oriented close to the line of sight. Alternatively, broad line emission can be a good indicator of thermal emission from the accretion process. Therefore, for our FSRQ sample, we estimate the black hole mass by using the empirical relation based on the luminosity and FWHM of broad emission lines. According to the source redshift, we use various relations to estimate the black hole mass: Vestergaard & Peterson (2006) for broad Hβ (see also Wu et al. 2004) and Kong et al. (2006) for broad Mg II and C IV lines.

For sources with available FWHM and luminosity of broad Hβ, the method to calculate $M_{\rm BH}$ is given by Vestergaard & Peterson (2006):

$$M_{\rm BH}({\rm H}\beta) = 4.68\times10^6 \left(\frac{L({\rm H}\beta)}{10^{42}\,{\rm erg\ s^{-1}}}\right)^{0.63} \left(\frac{{\rm FWHM}({\rm H}\beta)}{1000\,{\rm km\ s^{-1}}}\right)^2 M_\odot\,. \quad (4)$$

In addition, Kong et al. (2006) presented the empirical formula to obtain the black hole mass using broad Mg II and C IV for high redshift sources as follows,

$$M_{\rm BH}({\rm Mg\ II}) = 2.9\times10^{6}\left(\frac{L({\rm Mg\ II})}{10^{42}\,{\rm erg\,s^{-1}}}\right)^{0.57\pm0.12}\left(\frac{\rm FWHM(Mg\ II)}{1000\,{\rm km\,s^{-1}}}\right)^{2} M_{\odot}\,, \quad (5)$$

$$M_{\rm BH}({\rm C\ IV}) = 4.6\times10^{5}\left(\frac{L({\rm C\ IV})}{10^{42}\,{\rm erg\,s^{-1}}}\right)^{0.60\pm0.16}\left(\frac{\rm FWHM(C\ IV)}{1000\,{\rm km\,s^{-1}}}\right)^{2} M_{\odot}\,. \quad (6)$$

In the redshift range of our 14 FSRQs, $M_{\rm BH}$ can be estimated using two of the above relations for 7 sources, in which two $M_{\rm BH}$ values are consistent with each other within a factor of three. Therefore, we adopt the average value of the two estimates.

In this work, we estimate the BLR luminosity $L_{\rm BLR}$ following Celotti et al. (1997) by scaling the strong broad emission lines Hβ, Mg II and C IV to the quasar template spectrum of Francis et al. (1991), in which Lyα is used as a reference of 100. By adding the contribution of Hα with a value of 77, the total relative BLR flux is 555.77, of which Hβ is 22, Mg II 34, and C IV 63 (Celotti et al. 1997; Francis et al. 1991). From the BLR luminosity, we estimate the bolometric luminosity as $L_{\rm bol} = 10L_{\rm BLR}$ (Netzer 1990). The black hole mass, BLR luminosity and the Eddington ratio $L_{\rm bol}/L_{\rm Edd}$ are shown in Table 5.

Table 5 Black Hole Mass and BLR Luminosity

SDSS Name	log $M_{\rm BH}$ ($M_{\odot}$)	log $L_{\rm BLR}$ (erg s^{-1})	log $L_{\rm bol}$ (erg s^{-1})	log $L_{\rm bol}/L_{\rm Edd}$	log $L'_{\rm BLR}$ (erg s^{-1})
(1)	(2)	(3)	(4)	(5)	(6)
J082447.24+555242.6	9.49	46.04	47.04	–0.56	...
J092058.46+444154.0	9.88	47.04	48.04	0.05	...
J094857.33+002225.5	8.26	44.44	45.44	–0.93	44.39[a]
J095738.19+552257.7	9.20	45.11	46.11	–1.20	...
J101603.14+051302.3	9.78	46.00	47.00	–0.89	...
J103351.42+605107.3	9.39	45.25	46.25	–1.25	...
J105829.60+013358.8	9.25	45.32	46.32	–1.04	...
J115931.84+291443.8	9.11	45.30	46.30	–0.92	45.22[a]
J131028.66+322043.7	8.94	45.39	46.39	–0.66	44.72[a]
J150424.98+102939.1	9.50	46.36	47.36	–0.25	46.23[b]
J155332.69+125651.7	9.19	45.88	46.88	–0.42	...
J163515.50+380804.4	9.74	46.71	47.71	–0.14	46.53[b]
J164147.54+393503.3[L]	9.19	44.80	45.80	–1.50	44.74[a]
J222940.09-083254.5	9.40	46.36	47.36	–0.15	46.13[b]

Col. (1): SDSS name. [L] represents low-confidence association AGNs. Col. (2): the black hole mass. Col. (3): BLR luminosity. Col. (4): bolometric luminosity. Col. (5): the Eddington ratio. Col. (6): BLR luminosity estimated from single line ([a] for Hβ, [b] for Mg II).

3 RESULTS AND DISCUSSION

In Abdo et al. (2009a), the combination of the figure of merit approach (FoM) and positional association methods yields a number of 106 high-confidence (probability $P \geq 0.90$) associations (constituting the LBAS) and 11 low-confidence ($0.40 < P < 0.90$) associations. These 11 low-confidence associated Bright AGNs consist of 3 FSRQs, 2 BL Lacs, and 6 sources with uncertain classification, of which all have a flat radio spectrum but there are no other data reported in the literature allowing their classification either as FSRQs or BL Lacs. For γ-ray source 0FGL J1034.0+6051, two radio associations were found by the FoM method, one with very high probability ($P = 0.99$) and one with lower, but still significant, probability ($P = 0.79$). Although the high-probability source likely dominates the γ-ray emission, it is entirely plausible that the low-probability source contributes non-negligibly to the total γ-ray flux (Abdo et al. 2009a). In this work, SDSS data are only available for the high-confidence association

(see Table 1), from which the emission line measurements are given in Table 4 (also see Table 5). As stated in Abdo et al. (2009a), the early results from the first three months of the science mission of the *Fermi* Gamma ray Space Telescope demonstrate its exceptional capabilities to provide important new knowledge about γ-ray emission from AGNs and blazars. As the *Fermi*-LAT data accumulate, many more AGNs at lower flux levels will likely be detected, helping to improve our understanding of supermassive black holes (Abdo et al. 2009a). As predicted from AGN feedback by Wang (2008), there is extended faint gamma-ray fuzz around radio-quiet quasars, or red quasars. The *Fermi* Gamma ray Space Telescope is anticipated to explore the fuzz more feasibly. There is no doubt that the detection of the fuzz will provide the most powerful diagnostic to the evolutionary chains of galaxies and quasars from details of radiative feedback (see Wang 2008).

Radio-loud quasars, particularly FSRQs, differ from radio-quiet AGNs in the contribution of non-thermal jet emission in optical continuum emission, in addition to the thermal emission from the accretion disk. In particular, jet emission can be dominant due to the beaming effect when the jet is moving towards us with a small viewing angle. Indeed, Liu et al. (2006) found that the 5100 Å continuum luminosity for FSRQs generally exceeds that expected from the relationship between the 5100 Å continuum and broad Hβ luminosity for radio-quiet AGNs (see also Gu et al. 2009b). To inspect our FSRQs in a similar way, we investigate the relationship between the 3000 Å continuum and broad Mg II line luminosity, since the Mg II line is available and measured for most sources. The calibration of this relation is firstly performed for a sample of radio-quiet AGNs with reverberation mapping black hole mass (Kaspi et al. 2000) by collecting the relevant data in Kong et al. (2006). The ordinary least-square bisector linear fit gives:

$$\log \lambda L_{\lambda 3000\,\mathring{\rm A}} = (0.996 \pm 0.048) \log L_{\rm Mg\ II} + (1.895 \pm 2.024)\,, \tag{7}$$

which is plotted in Figure 2, as well as the data points of radio-quiet AGNs.

The relationship between the broad Mg II luminosity and luminosity at 3000 Å for our FSRQs is shown in Figure 2. When the Mg II line is not available, we calibrate the C IV line to the Mg II line adopting the relative flux (Mg II=34, C IV=63) of the relevant lines of the composite spectrum of Francis et al. (1991). The luminosity at 3000 Å is calculated from the power-law fit on the spectral continuum. From Figure 2, it can be seen that the 3000 Å luminosity of most sources lies above the $\lambda L_{\lambda 3000\,\mathring{\rm A}} - L_{\rm Mg\ II}$ relation of radio-quiet AGNs. However, the deviation of $\lambda L_{\lambda 3000\,\mathring{\rm A}}$ is within one order of magnitude. The average value of $\lambda L_{\lambda 3000\,\mathring{\rm A}}/L_{\rm Mg\ II}$ is $\langle \log (\lambda L_{\lambda 3000\,\mathring{\rm A}}/L_{\rm Mg\ II}) \rangle = 1.73 \pm 0.24$ for radio-quiet AGNs, while it is $\langle \log (\lambda L_{\lambda 3000\,\mathring{\rm A}}/L_{\rm Mg\ II}) \rangle = 2.21 \pm 0.27$ for our FSRQs. Therefore, the $\lambda L_{\lambda 3000\,\mathring{\rm A}}$ of our FSRQs is, on average, higher than that of radio-quiet AGNs by a factor of three at a given $L_{\rm Mg\ II}$, which is most likely due to the non-thermal jet emission. As expected for FSRQs, this implies that the non-thermal jet emission in FSRQs generally can be dominant over thermal emission, with the former likely being Doppler boosted. Adopting a Doppler factor of $\delta = 10$, typical for FSRQs (Ghisellini et al. 1998; Jiang et al. 1998; Gu et al. 2009a), and assuming the corresponding Doppler boosting $\delta^{2+\alpha}$ (corresponding to a continuous jet, α is the spectral index) in jet emission, the intrinsic jet emission in the optical band, however, can be much smaller than the thermal emission (mainly from the accretion disk) for our FSRQs. However, the dependence of the Doppler factor on the frequency has been proposed (Zhang et al. 2002), with a lower Doppler factor ~ 5 claimed in the optical region. In contrast, Chen et al. (2009) showed that the thermal emission from the accretion disk and the host galaxy can be dominant in 67 out of 185 FSRQs ($\sim 36\%$) selected from the SDSS DR 3 quasar catalog. As Landt et al. (2008) claimed, the flat radio spectrum does not prove jet-dominance in continuum emission. The high radio core-dominance, in addition to a flat radio spectrum, are proposed to find jet-dominant FSRQs. We note that the $\lambda L_{\lambda 3000\,\mathring{\rm A}} - L_{\rm Mg\ II}$ relation of radio-quiet AGNs is established from a relatively low luminosity, which does not cover the luminosity range of our FSRQs. Further investigations are needed.

It can be seen from Table 5 that the black hole masses of 14 FSRQs range from $10^{8.2}\,M_\odot$ to $10^{9.9}\,M_\odot$, with most sources larger than $10^9\,M_\odot$. The BLR luminosity varies from $10^{44.44}$ erg s^{-1} to $10^{47.04}$ erg s^{-1}. The Eddington ratio $L_{\rm bol}/L_{\rm Edd}$ ranges from $10^{-1.5}$ to ~ 1. This implies that an

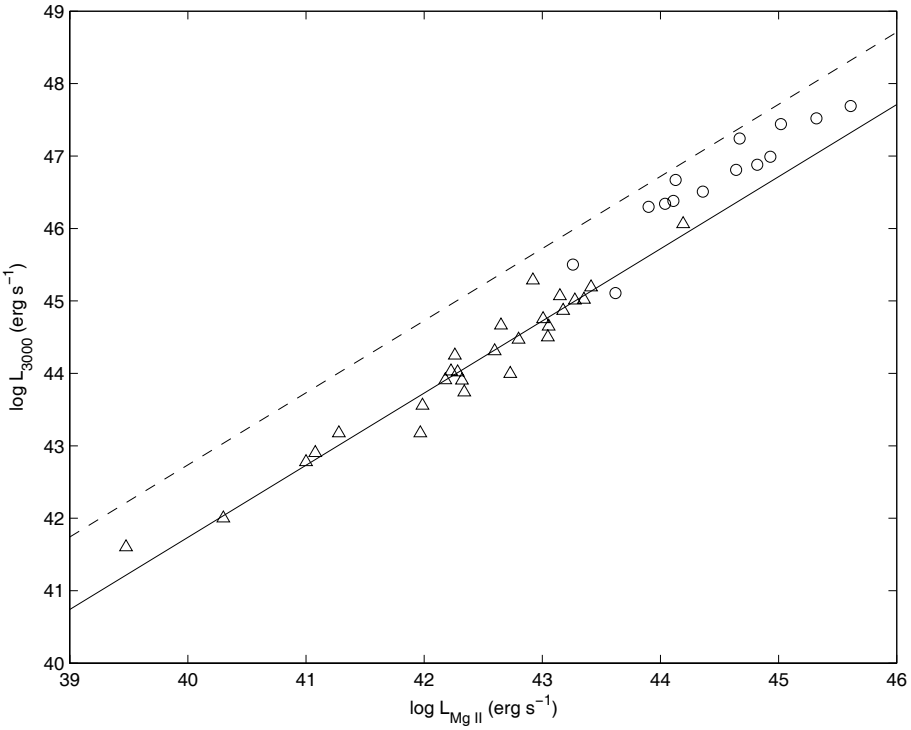

Fig. 2 Luminosity at 3000 Å versus broad Mg II luminosity. The open circles are our FSRQs, while open triangles represent the radio-quiet AGNs in Kong et al. (2006). The solid line is the OLS bisector linear fit to radio-quiet AGNs in Kong et al. (2006), $\lambda L_{\lambda 3000\,\mathrm{\AA}} = 78.5\ L_{\mathrm{Mg\ II}}^{0.996}$ (see Eq. (7)). The dashed line represents the deviation from the solid line by one order of magnitude in $\lambda L_{\lambda 3000\,\mathrm{\AA}}$, which is used to indicate the deviation of our FSRQs from the relation for radio-quiet AGNs.

optically thin, geometric thick accretion disk (Shakura & Sunyaev 1973) may exist in these FSRQs. This is consistent with the radio-loud quasars in Wang et al. (2003), of which the accretion rates $\dot{M} \approx 0.01-1$ times the Eddington rate, suggesting that most sources possess standard optically thick, geometrically thin accretion disks. In contrast, the accretion mode in BL Lacs is not homogeneous, with standard thin disks probably in luminous BL Lacs, and advection-dominated accretion flows in less luminous ones (e.g. Cao 2002). Moreover, the evolutionary sequence of blazars, from FSRQs to low-energy-peaked BL Lac objects to high-energy-peaked BL Lac objects, is suggested along the decreasing accretion rate (e.g. Cao 2002; Cavaliere & D'Elia 2002; Wang et al. 2003). While we estimate the BLR luminosity from multiple emission lines following Celotti et al. (1997), it is argued that the BLR luminosity can be better derived from a single line than multiple lines due to the very large scatter in the ratio of some key lines (e.g. C IV and Mg II) with respect to Ly α (Wang et al. 2004). Following the suggestion of Wang et al. (2004), for seven of our FSRQs with multiple line measurements (see Table 4), we re-estimated the BLR luminosity using only the Hβ line, or Mg II when Hβ is not available, which is listed in Table 5. We find that the BLR luminosity from a single line is consistent with that from multiple lines within a factor of two, except for SDSS J131028.66+322043.7, with the former smaller than the latter by a factor of 4.7 (see Table 5). This implies that the relative fluxes of Hβ, Mg II and C IV, at least for these seven FSRQs, generally follow the Francis et al. (1991) composite spectrum, although they are strong γ-ray and radio sources. Apparently, using a single line does not significantly alter the Eddington ratio estimates.

Our BLR measurements can be used in further investigations relevant to *Fermi* γ-ray emission. For example, the model fit to SEDs, including external Compton processes and SSC, will be presented for LBAS sources in a future paper (Li et al., in preparation), in which the BLR measurements in this paper can be used to constrain the energy density of BLR emission in jets. Moreover, to investigate the mechanism of γ-ray emission, the work of Fan et al. (2006), will be re-investigated for LBAS sources by using our BLR measurements and collecting BLR measurements from the literature (Fan et al. in preparation). As a matter of fact, the BLR data for five FSRQs (SDSS J082447.24+555242.6, SDSS J094857.33+002225.5, SDSS J101603.14+051302.3, SDSS J155332.69+125651.7 and SDSS J222940.09–083254.5) are not available from the literature, and are, therefore, measured and provided for the first time in this paper (see Table 4). Despite an extensive literature search, the BLR measurements are still not available for some LBAS sources; therefore, the spectroscopic observations are needed since the external Compton processes from BLR seed photons are thought to be primary for γ-ray emission (Fan et al. 2006).

Acknowledgements We thank the anonymous referee for insightful comments and constructive suggestions. This work is supported by the National Natural Science Foundation of China (Grant Nos. 10633010, 10703009, 10833002, 10773020 and 10821302), the 973 Program (No. 2009CB824800), and the CAS (KJCX2-YW-T03). ZHF is supported by the Yunnan Provincial Science Foundation of China (grant 2008CD061). This research made use of the NASA/IPAC Extragalactic Database (NED), which is operated by the Jet Propulsion Laboratory, California Institute of Technology, under contract with the National Aeronautics and Space Administration.

Funding for the SDSS and SDSS-II has been provided by the Alfred P. Sloan Foundation, the Participating Institutions, the National Science Foundation, the U.S. Department of Energy, the National Aeronautics and Space Administration, the Japanese Monbukagakusho, the Max Planck Society, and the Higher Education Funding Council for England. The SDSS Web Site is *http://www.sdss.org/*.

The SDSS is managed by the Astrophysical Research Consortium for the Participating Institutions. The Participating Institutions are the American Museum of Natural History, Astrophysical Institute Potsdam, University of Basel, University of Cambridge, Case Western Reserve University, University of Chicago, Drexel University, Fermilab, the Institute for Advanced Study, the Japan Participation Group, Johns Hopkins University, the Joint Institute for Nuclear Astrophysics, the Kavli Institute for Particle Astrophysics and Cosmology, the Korean Scientist Group, the Chinese Academy of Sciences (LAMOST), Los Alamos National Laboratory, the Max-Planck-Institute for Astronomy (MPIA), the Max-Planck-Institute for Astrophysics (MPA), New Mexico State University, Ohio State University, University of Pittsburgh, University of Portsmouth, Princeton University, the United States Naval Observatory, and the University of Washington.

References

Abdo, A. A., et al. 2009a, ApJ, 700, 597
Abdo, A. A., et al. 2009b, ApJS, 183, 46
Cao, X. W. 2002, ApJ, 570, L13
Cavaliere, A., & D'Elia, V. 2002, ApJ, 571, 226
Celotti, A., Padovani, P., & Ghisellini, G. 1997, MNRAS, 286, 415
Chen, Z. Y., Gu, M. F., & Cao, X. 2009, 397, 1713
Collmar, W., Reimer, O., Bennett, K., et al. 2000, A&A, 354, 513
Dietrich, M., Appenzeller, I., Vestergaard, M., & Wagner, S. J. 2002, ApJ, 564, 581
Fan, J. H. 2000, A&A, 358, 841
Fan, Z. H., Cao, X. W., & Gu, M. F. 2006, ApJ, 646, 8
Forster, K., Green, P. J., Aldcroft, T. L., Vestergaard, M., Foltz, C. B., & Hewett, P. C. 2001, ApJS, 134, 35
Francis, P. J., Hewett, P. C., Foltz, C. B., Chaffee, F. H., Weymann, R. J., & Morris, S. L. 1991, ApJ, 373, 465
Ghisellini, G., Celotti, A., Fossati, G., Maraschi, L., & Comastri, A. 1998, MNRAS, 301,451
Ghisellini, G., & Tavecchio, F. 2008, MNRAS, 387, 1669

Grandi, S. A. 1982, ApJ, 255, 25
Gu, M. F., Cao, X., & Jiang, D. R. 2009a, MNRAS, 396, 984
Gu, M. F., Chen, Z. Y., & Cao, X. 2009b, MNRAS, 397, 1705
Jiang, D. R., Cao, X., & Hong, X. 1998, ApJ, 494, 139
Kaspi, S., Smith, P. S., Netzer, H., Maoz, D., Jannuzi, B. T., & Giveon, U. 2000, ApJ, 533, 631
Kim, M., Ho, L. C., & Im, M. 2006, ApJ, 642, 702
Kong, M. Z., Wu, X. B., Wang, R., & Han, J. L. 2006, ChJAA (Chin. J. Astron. Astrophys.), 6, 396
Landt, H., Padovani, P., & Giommi, P. 2002, MNRAS, 336, 945
Landt, H., Padovani, P., Giommi, P., Perri, M., & Cheung, C. C. 2008, ApJ, 676, 87
Liu, Y., Jiang, D. R., & Gu, M. F. 2006, ApJ, 637, 669
Marchã, M. J. M., Browne, I. W. A., Impey, C. D., & Smith, P. S. 1996, MNRAS, 281, 425
Netzer, H. 1990, in Active Galactic Nuclei, ed. R. D. Blandford et al. (Berlin: Springer), 57
Oke, J. B., & Gunn, J. E. 1983, ApJ, 266, 713
Padovani, P., & Giommi, P. 1995, ApJ, 444, 567
Rector, T. A., & Stocke, J. T. 2001, AJ, 122, 565
Schlegel, D. J., Finkbeiner, D. P., & Davis, M. 1998, ApJ, 500, 525
Shakura, N. I., & Sunyaev, R. A. 1973, A&A, 24, 337
Stickel, M., Padovani, P., Urry, C. M., Fried, J. W., & Kühr, H. 1991, ApJ, 374, 431
Vanden Berk, D. E., Richards, G. T., Bauer, A., Strauss, M. A., et al. 2001 AJ, 122, 549
Véron-Cetty, M. P., Joly, M., & Véron, P. 2004, A&A, 417, 515
Vestergaard, M., & Peterson, B. M. 2006 ApJ, 641, 689
Vestergaard, M., & Wilkes, B. J. 2001, ApJS, 134, 1
Wang, J. M. 2008, ApJ, 682, L81
Wang, J. M., Ho, L. C., & Staubert, R. 2003, A&A, 409, 887
Wang, J. M., Luo, B., & Ho, L. C. 2004, ApJ, 615, L9
Wehrle, A. E., Pian, E., Urry, C. M., et al. 1998, ApJ, 479, 178
Wu, X. B., Wang, R., Kong, M. Z., Liu, F. K., & Han, J. L. 2004, A&A, 424, 793
Zhang, L., Fan, J. H., & Cheng, K. S. 2002, PASJ, 54, 159